Multispacecraft observations of fundamental poloidal waves without ground magnetic signatures

Kazue Takahashi,[1] Michael D. Hartinger,[2] Vassilis Angelopoulos,[3]
Karl-Heinz Glassmeier,[4,5] and Howard J. Singer[6]

Received 27 March 2013; revised 14 June 2013; accepted 17 June 2013; published 24 July 2013.

[1] Poloidal standing Alfvén waves observed by spacecraft usually have a second harmonic standing wave structure. On very rare occasions, fundamental poloidal waves have been observed in association with giant pulsations observed on the ground. In this paper, we report multisatellite observations of fundamental poloidal waves that did not produce any clearly associated magnetic pulsations on the ground. The waves were observed on 10 November 2008, at ~1830 Universal Time (UT) at THEMIS-A and THEMIS-D and at ~2010 UT at THEMIS-E as these spacecraft passed $L \sim 11$ and magnetic local time (MLT) ~ 0900. The GOES-11 geostationary satellite ($L \sim 7$) also observed poloidal waves at ~1730 UT when it was at ~0900 MLT. The poloidal waves at THEMIS were characterized by narrow-band oscillations (frequency ~4 mHz) of the ion bulk velocity and magnetic field in the radial direction. We identify the waves at THEMIS to be the fundamental mode on the basis of the wave properties observed slightly south of the magnetic equator: large velocity amplitude, small magnetic field amplitude, and ~90° phase delay of the magnetic field relative to the velocity. The azimuthal wave number is found to be ~70 (if we assume westward propagation) or ~200 (if we assume eastward propagation) from the phase delay between THEMIS-A and THEMIS-D. This wave number explains why there were no corresponding magnetic field oscillations on the ground. These observations imply that only a subset of fundamental poloidal waves excited in the magnetosphere is observed on the ground as giant pulsations.

Citation: Takahashi, K., M. D. Hartinger, V. Angelopoulos, K.-H. Glassmeier, and H. J. Singer (2013), Multispacecraft observations of fundamental poloidal waves without ground magnetic signatures, *J. Geophys. Res. Space Physics*, *118*, 4319–4334, doi:10.1002/jgra.50405.

1. Introduction

[2] The drift-bounce resonance mechanism is a very common process in the terrestrial magnetosphere causing the generation of ultralow frequency (ULF) waves [*Southwood et al*., 1969; *Hughes et al*., 1978]. Depending on the actual energy of the resonant particle, this mechanism gives rise to ULF waves with a broad range of azimuthal wave numbers, *m* values [e.g., *Ozeke and Mann*, 2001]. At the ground, so-called giant pulsations (Pgs) have been suggested to be a witness of this resonant excitation process [*Glassmeier*, 1980; *Takahashi et al*., 1992]. Because of the ionospheric screening effect, only those resonant waves with not too large *m* values can be seen on the ground [e.g., *Hughes and Southwood*, 1976]. Accordingly, Pgs appear to be a subclass of the more general class of ULF waves generated by the drift-bounce mechanism. Here we analyze in more detail one of the members of large *m* ULF waves and demonstrate that its ground signature is absent. Thereby, we provide further evidence for the ionosphere acting as a filter for magnetospheric dynamics. The remainder of this section provides a brief historical background and a more specific description of the physical processes relevant to the waves.

1.1. Poloidal Standing Alfvén Waves

[3] Long-to-medium-period ULF waves in the magnetosphere, or Pc3–5 waves (period 10–600 s), are routinely observed and many of them are identified as standing Alfvén waves. The basic properties of the observed waves such as frequency and perturbations in the electric and magnetic fields are consistent with theoretical predictions for standing Alfvén waves [*Dungey*, 1954]. Currently, a

[1]The Johns Hopkins University Applied Physics Laboratory, Laurel, Maryland, USA.
[2]Department of Atmospheric, Oceanic and Space Sciences, University of Michigan, Ann Arbor, Michigan, USA.
[3]Institute of Geophysics and Planetary Physics and Department of Earth and Space Sciences, University of California, Los Angeles, California, USA.
[4]Institute for Geophysics and Extraterrestrial Physics, Technical University of Braunschweig, Braunschweig, Germany.
[5]Max Planck Institute for Solar System Research, Katlenburg-Lindau, Germany.
[6]Space Weather Prediction Center, National Centers for Environmental Prediction, National Weather Service, NOAA, Boulder, Colorado, USA.

Corresponding author: K. Takahashi, The Johns Hopkins University Applied Physics Laboratory, 11100 Johns Hopkins Rd., Laurel, MD 20723-6099, USA. (kazue.takahashi@jhuapl.edu)

2169-9380/13/10.1002/jgra.50405

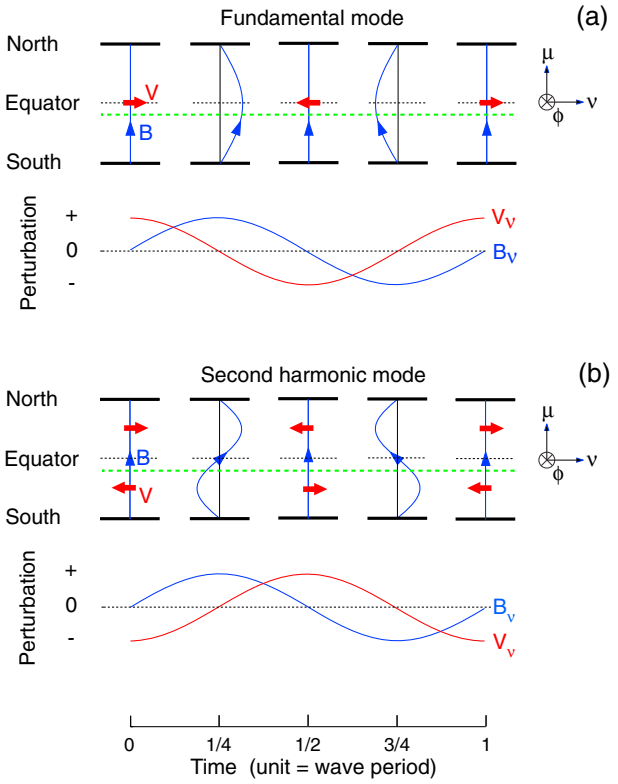

Figure 1. Illustration of poloidal standing Alfvén waves. Field lines are tied to the ionosphere at the southern and northern ends. In the upper part of each panel, field line displacement (blue line) and the associated plasma bulk speed (red arrow) are shown at four phases of an oscillation cycle. The coordinate axes are defined on the right. The horizontal dashed line, drawn slightly south of the magnetic equator, represents the location of the THEMIS spacecraft for the observations described in the main text. In the lower part, the temporal variations of V_ν and B_ν are shown for one oscillation cycle to explain the phase lag between them. (a) Fundamental mode. (b) Second harmonic mode.

major goal in studying these waves is to understand how they are excited and interact with magnetospheric particles. In general, standing Alfvén waves can be excited either by disturbances external to the magnetosphere (such as solar dynamic pressure variations) or by plasma instabilities within the magnetosphere. In this paper, we are concerned with internal mechanisms.

[4] Internally excited standing Alfvén waves are characterized by strong magnetic field perturbations in the radial (poloidal) direction. Compared with toroidal waves [*Radoski and Carovillano*, 1966], which have strong azimuthal magnetic field perturbations and are usually attributed to external source mechanisms [*Chen and Hasegawa*, 1974; *Southwood*, 1974], poloidal waves have a large value of m (with minus sign indicating westward propagation), which can be on the order of 100. In the limit of $|m| = \infty$, the cold plasma magnetohydrodynamic (MHD) wave equations for a dipole magnetic field yield a solution called the guided poloidal mode [*Radoski*, 1967]. The frequency and variation of the electric and magnetic field perturbations along the field line facilitate the harmonic mode identification of the observed poloidal ULF waves. When the plasma pressure is high, the poloidal waves are accompanied by a strong magnetic field compressional component, which tends to be balanced with the plasma pressure oscillations [*Southwood*, 1976; *Chen and Hasegawa*, 1991; *Cheng and Qian*, 1994]. Note that compressional poloidal waves with low $|m|$ values are also observed and are known as global modes [e.g., *Kivelson et al.*, 1984; *Hartinger et al.*, 2013]. Global mode waves have a strong fast mode component and their properties are determined by the radial structure of the plasma mass density and Alfvén speed. Global poloidal waves are outside the scope of the present paper.

1.2. Field Line Harmonic Mode and Excitation Mechanism

[5] One property that is important in understanding the excitation mechanism of poloidal waves is the field line harmonic mode. Because much of the present paper is devoted to describing observational evidence of fundamental poloidal waves, we show in Figure 1 an illustration of key observable features of the waves and contrast them with those of the second harmonic waves. The figure uses a straight equilibrium magnetic field line for the sake of simplicity [e.g., *Sugiura and Wilson*, 1964], which is adequate for qualitative description of field line mode structure and the phase relation between the plasma bulk velocity (**V**) and magnetic field (**B**). For the **V** and **B** vectors, the coordinate axes are taken along the direction of the unperturbed magnetic field (μ), radially outward (ν), and eastward (ϕ). The figure is similar to those used previously in studies of standing Alfvén waves [*Cummings et al.*, 1978; *Singer et al.*, 1982; *Takahashi et al.*, 2011].

[6] The fundamental (Figure 1a) and second harmonic (Figure 1b) modes can be distinguished in various ways. For example, one can rely on the fact that the magnetic equator is the location of the antinode (maximum amplitude) of field line displacement for the fundamental mode, whereas it is the location of the node (zero amplitude) for the second harmonic. Therefore, if we observe a large (small) V_ν oscillation near the magnetic equator, the oscillation probably has a fundamental (second harmonic) mode structure. This is the reverse for the B_ν oscillation (note that the B_ν amplitude is proportional to the tilt angle of the field line). Also, the phase delay between V_ν and B_ν differs between the fundamental and second harmonic modes. For the fundamental (second harmonic) mode measured slightly south of the magnetic equator (indicated by the horizontal dashed line), V_ν leads (lags) B_ν by 90°.

[7] Observations indicate that poloidal waves are excited mostly at the second harmonic [*Cummings et al.*, 1969; *Hughes et al.*, 1978; *Arthur and McPherron*, 1981; *Singer et al.*, 1982; *Takahashi and McPherron*, 1984; *Engebretson et al.*, 1988]. Second harmonic poloidal waves are common even when there is a strong compressional component in the magnetic field [*Takahashi et al.*, 1987; *Haerendel et al.*, 1999; *Vaivads et al.*, 2001; *Sibeck et al.*, 2012]. Theory offers explanations for the preferential excitation of the second harmonic mode in the ring current environment [*Southwood*, 1976; *Chen and Hasegawa*, 1991; *Cheng and Qian*, 1994; *Chan et al.*, 1994]. A popular scenario is that ring current ions forming a bump-on-tail energy distribution

(usually in the 5–50 keV energy range) feed energy to the waves through the drift-bounce resonance

$$\omega - m\omega_d = N\omega_b. \quad (1)$$

[8] Here ω is wave frequency, ω_d and ω_b are the guiding center drift and bounce frequencies of the ions, and N is an integer that we call bounce harmonic number [*Southwood et al*., 1969; *Southwood*, 1976; *Hughes et al*., 1978; *Chisham*, 1996; *Baddeley et al*., 2004, 2005; *Wilson et al*., 2006]. The symmetry (odd or even) of the standing wave about the magnetic equator dictates which bounce harmonic is relevant [*Southwood and Kivelson*, 1982]. For odd mode (e.g., fundamental) waves, N is even, and for even mode (e.g., second harmonic) waves, N is odd. For the case of the second harmonic standing waves, $N = \pm 1$ is the most likely bounce harmonic that channels energy between particles and waves [*Southwood*, 1976].

[9] Although very rare, fundamental poloidal waves have been reported. *Yang et al*. [2010] reported a storm-time transient event observed by CLUSTER satellites. *Eriksson et al*. [2005] reported three high-m odd-mode poloidal wave events, also observed by CLUSTER, and the authors discussed the possibility of the waves being either the fundamental or the third harmonic standing waves. Besides these, satellite observations of fundamental poloidal waves are limited to those associated with Pgs observed on the ground, usually in the Pc4 band (period = 45–150 s). Pgs are rare phenomena that occur approximately 20 times a year in the late declining phase of the solar activity but are essentially nonexistent at the peak of the solar activity [*Brekke et al*., 1987]. Other unique features of Pgs include a highly monochromatic waveform, a strong east-west ground magnetic field perturbation, localization around dawn and at $L \sim 6$, and peak occurrence at the equinoxes under quiet geomagnetic conditions [*Rostoker et al*., 1979; *Glassmeier*, 1980; *Hillebrand et al*., 1982; *Poulter et al*., 1983; *Chisham and Orr*, 1991]. Because Pgs are uniquely identified only on the ground, studies of magnetospheric source waves for Pgs need to start from event identification on the ground.

[10] In a recent study, *Takahashi et al*. [2011] combined electric and magnetic field data from a THEMIS spacecraft and magnetic field data from four GOES geostationary spacecraft to demonstrate that 100-s poloidal waves associated with Pgs on the ground had a fundamental mode structure. This result confirmed earlier studies that used single-satellite observations [*Kokubun*, 1980; *Hillebrand et al*., 1982; *Kokubun et al*., 1989; *Takahashi et al*., 1992; *Glassmeier et al*., 1999].

1.3. Ionospheric Screening

[11] We are intrigued by the fact that Pgs are well-defined phenomena yet they occur so infrequently. Why are they so rare? What special magnetospheric condition is required for their excitation? To answer these questions, it is necessary to improve our understanding of the occurrence morphology of fundamental poloidal waves in the magnetosphere. This is because Alfvén waves with a small latitudinal scale [e.g., *Glassmeier and Stellmacher*, 2000] or a high $|m|$ value [*Wright and Yeoman*, 1999; *Yeoman and Wright*, 2001] are screened by the ionosphere and do not produce detectable magnetic pulsations on the ground. According to *Hughes and Southwood* [1976] and *Glassmeier* [1984], the attenuation factor A of Alfvén wave amplitude through the ionosphere is given by

$$A \sim (\Sigma_H/\Sigma_P)\exp(-2\pi h/\lambda_\phi), \quad (2)$$

where Σ_H and Σ_P are the height-integrated Hall and Pedersen conductivities, respectively, h is the effective height (~120 km) of the ionosphere, and λ_ϕ is the azimuthal wavelength at the ionospheric height. If $\Sigma_H \sim \Sigma_P$ and the wavelength is comparable to or shorter than the ionospheric height, $\lambda_\phi < h$, then there will be a very strong attenuation, $A < 10^{-3}$.

[12] Previously reported Pgs had $|m|$ values smaller than 35 [*Rostoker et al*., 1979], but there is no a priori reason that the same mechanism that generates Pgs cannot generate high-m ($|m| > 35$) poloidal waves that are screened out by the ionosphere. Namely, Pgs may be a manifestation of a small subset of fundamental poloidal waves excited in the magnetosphere. This possibility is well founded in view of simultaneous high-frequency (HF) radar and ground magnetometer observations of ULF pulsations [*Yeoman and Wright*, 2001].

1.4. Organization of the Paper

[13] This paper combines data from three THEMIS spacecraft, one GOES satellite, and ground magnetometers close to the magnetic field foot points of the satellites to demonstrate that fundamental poloidal waves occurred in the magnetosphere without producing any corresponding magnetic pulsations on the ground. The overall data analysis approach is quite similar to that used by *Takahashi et al*. [2011] for a Pg event except that in the present study, we have two THEMIS spacecraft very close to each other, which allows us to determine the azimuthal wave number. As expected, we find that the azimuthal wave number of the poloidal waves is high, with $|m| \sim 70$ or ~200. Although such events are very rare, this result nevertheless indicates that fundamental poloidal waves occur in the magnetosphere without producing Pg signals on the ground. In this paper, we focus on wave mode analysis and leave examination of particle distribution functions for future studies.

[14] The remainder of the paper is organized as follows. Section 2 describes the experiments used to acquire data used for this study. Section 3 presents an overview of the observations. Section 4 presents THEMIS data. Section 5 examines GOES data. Section 6 compares waves in the magnetosphere and magnetic field variations on the ground. Section 7 presents discussion. Section 8 presents the conclusions.

2. Experiments

[15] The THEMIS-A, THEMIS-D, and THEMIS-E spacecraft are the main source of data used in the present study. At the time of the wave event reported here, the spacecraft were in nearly identical orbits with apogees around 12 R_E geocentric. To study ULF waves, we use the ion bulk velocity vector **V** calculated on board at the cadence of the spacecraft spin period (~3 s) from the ion flux measured by the electrostatic analyzer (ESA) in the energy range 5 eV –25 keV [*McFadden et al*., 2008] and the magnetic field vector **B** measured by the fluxgate magnetometer [*Auster et al*., 2008], also processed into the spin period time

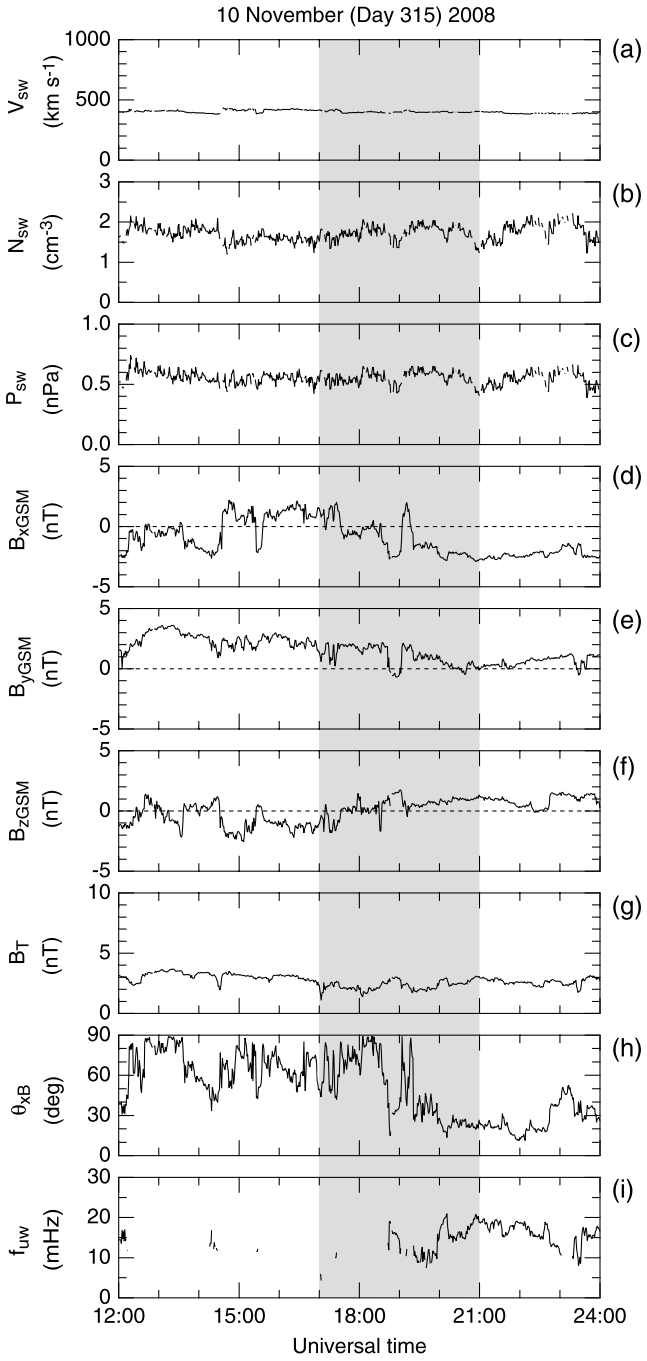

Figure 2. Time-shifted OMNI solar wind data in 1 min resolution covering the second half of 10 November 2008. Poloidal waves were observed by the THEMIS and GOES spacecraft during the 4 h period highlighted by shading. The (c) dynamic pressure P_{sw} was calculated from the (a) flow speed V_{sw} and (b) density N_{sw}. The (h) IMF cone angle θ_{xB} was calculated from the (d–g) measured magnetic field. The (i) upstream wave frequency f_{uw} was calculated using the measured magnetic field and the theoretical formula of *Takahashi et al*. [1984].

resolution. We have evaluated the contribution of ions with energy higher than 25 keV, measured by the solid state telescope (SST) [*Angelopoulos*, 2008], to the bulk velocity and found that it is negligible. We do not use the electric field data [*Bonnell et al*., 2008] because the satellite wake and asymmetric boom illumination strongly affected the measurement. The THEMIS data are supplemented by magnetic field data from the GOES-11 geostationary satellite [*Singer et al*., 1996] and the CARISMA [*Mann et al*., 2008] and THEMIS-Ground Based Observatory (GBO) [*Russell et al*., 2008] ground magnetometer arrays. Because the GOES and ground magnetometer data had an original time resolution of 1 s or higher, we reduced the resolution to 10 s (GOES) or 5 s (ground magnetometers) after taking running averages of the original data. In spectral analyses, we applied the Fourier transform [*Bendat and Piersol*, 1971] to the time series from which the best-fit second-order polynomial has been subtracted.

[16] To separate the toroidal and poloidal components of oscillations in **V** and **B**, we express these vectors in a model-field-aligned coordinate system. In this system, the compressional component $\mathbf{e}_\mu$ is along the magnetic field given by combining the International Geomagnetic Reference Field (IGRF) (http://www.ngdc.noaa.gov/IAGA) and the T89c [*Tsyganenko*, 1989] models, the eastward component $\mathbf{e}_\phi$ is given by $\mathbf{e}_\mu \times \mathbf{R}$ where **R** is the radial vector pointing from the center of the Earth toward the satellite, and the radial component $\mathbf{e}_\nu = \mathbf{e}_\phi \times \mathbf{e}_\mu$ completes the right-handed system $\nu - \phi - \mu$. During the poloidal wave event at each THEMIS spacecraft, the direction of the observed field was within 4° of the model field (the magnitude differs by up to 20%). Therefore, the model is satisfactory for the purpose of separating directions parallel and perpendicular to the background magnetic field.

3. Observational Background

[17] The waves were observed in the dayside magnetosphere between 1700 and 2100 UT on 10 November (day of year 315) 2008. This time was near the solar minimum. This section provides some background information for the wave event.

3.1. Solar Wind and Geomagnetic Condition

[18] Figure 2 shows the 1 min OMNI solar wind data [http://omniweb.gsfc.nasa.gov/ow_min.html] for the second half of 10 November 2008. The data have been time shifted to the bow shock. During the 4 h interval 1700–2100 UT (highlighted), which includes the poloidal wave activity at the THEMIS and GOES satellites, the solar wind velocity was steady at ~400 km/s (Figure 2a), the density varied between 1.3 and 2.1 cm^{-3} (Figure 2b), and the dynamic pressure calculated from the velocity and density was in the range of 0.4–0.7 Pa (Figure 2c). The interplanetary magnetic field (IMF) had a magnitude of 1–3 nT (Figure 2g), and its z component in the geocentric solar magnetospheric (GSM) coordinates was mostly near zero or positive (Figure 2f). The IMF cone angle, $\theta_{xB} = \cos^{-1}(|B_{xGSM}|/B_t)$, varied significantly between ~30° and ~90° (Figure 2h), and the frequency of upstream waves f_{uw}, calculated using the formula of *Takahashi et al*. [1984] and shown only when $\theta_{xB} < 45°$, was in the range of 10–20 mHz (Figure 2i).

[19] Figure 3 shows geomagnetic activity indices provided by the World Data Center for Geomagnetism, Kyoto [http://wdc.kugi.kyoto-u.ac.jp] covering the poloidal wave event. In each panel, the shading indicates the 4 h period

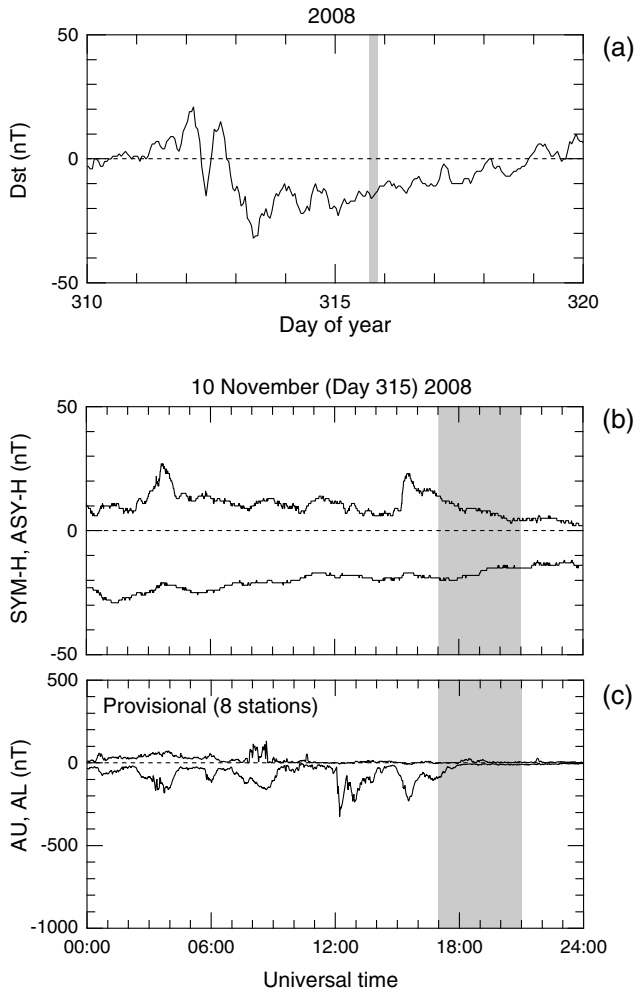

Figure 3. Geomagnetic indices covering a 4 h period of poloidal wave activity (highlighted by shading). (a) *Dst* index for 10 days. (b) Ring current indices *SYM-H* and *ASY-H* for 10 November 2008. (c) Auroral electrojet indices AU and AL for 10 November 2008.

of interest. Figure 3a shows that there was a minor development in ring current intensity leading to a *Dst* minimum of −32 nT on day 313 (8 November). The waves occurred during the recovery phase of this very small geomagnetic storm. Figures 3b and 3c show that there were substorms on day 315. The AL index shows a sharp decrease at ~1200 UT to the minimum of −326 nT and a less abrupt decrease at ~1500 UT to the minimum of −231 nT. During the time period of the poloidal waves, there was no substorm activation.

3.2. Spacecraft Orbits

[20] Figure 4a shows the orbits of the THEMIS-A, THEMIS-D, and THEMIS-E spacecraft and the geostationary GOES-11 satellite for the whole day of 10 November 2008, projected on the geocentric solar ecliptic (GSE) *X*–*Y* plane. The THEMIS spacecraft were on nearly identical orbits but with a time delay: THEMIS-D trailed THEMIS-A by ~40 min and THEMIS-E trailed THEMIS-D by ~90 min. The thick portions of the orbits indicate where the waves were observed. At the THEMIS spacecraft, the poloidal

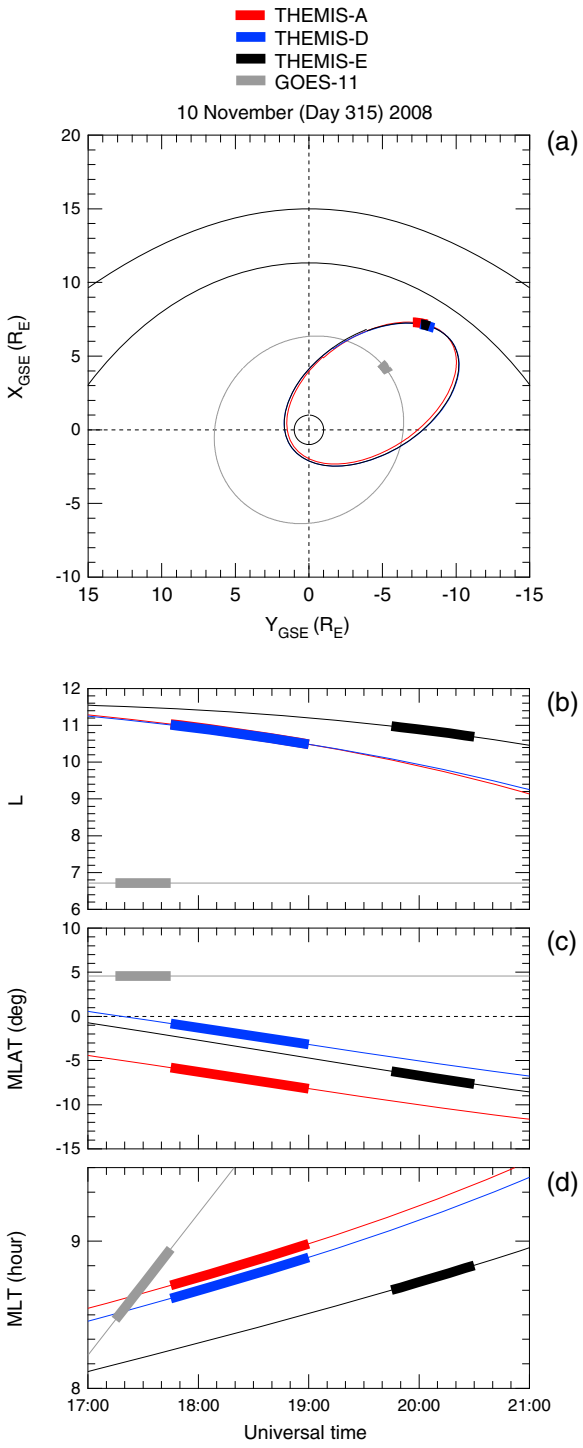

Figure 4. (a) GSE *X* and *Y* positions of THEMIS-A, THEMIS-D, THEMIS-E, and GOES-11 on 10 November 2008. The thick segments of the orbit indicate where poloidal waves were observed. A realistic magnetopause position is given by the *Shue et al.* [1998] model for solar wind dynamic pressure of 0.7 Pa and IMF GSM *z* component of –2 nT. The bow shock location is given by *Fairfield* [1971]. (b) Dipole-based magnetic field coordinates, *L* (field line equatorial distance normalized to the Earth radius), (c) MLAT (magnetic latitude in degrees), and (d) MLT (magnetic local time in hours) of the four spacecraft from 1700 to 2100 UT. The thick line segments indicate poloidal wave activity.

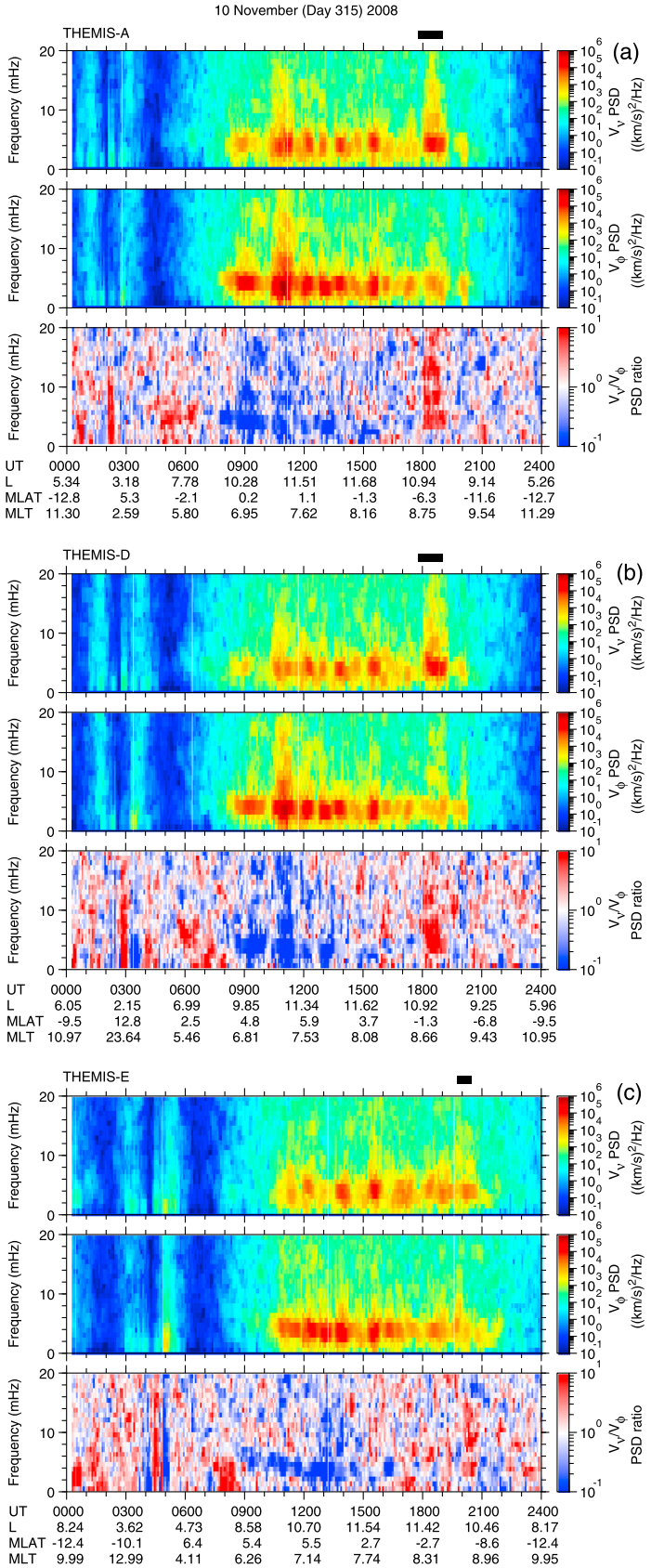

Figure 5. Dynamic spectra of (top) V_v and (middle) V_ϕ and (bottom) the V_v-to-V_ϕ power ratio at THEMIS spacecraft for 10 November 2008. The power ratio is color coded such that stronger V_v (V_ϕ) power appears red (blue). The short horizontal bars indicate the poloidal waves described in the text. (a) THEMIS-A. (b) THEMIS-D. (c) THEMIS-E.

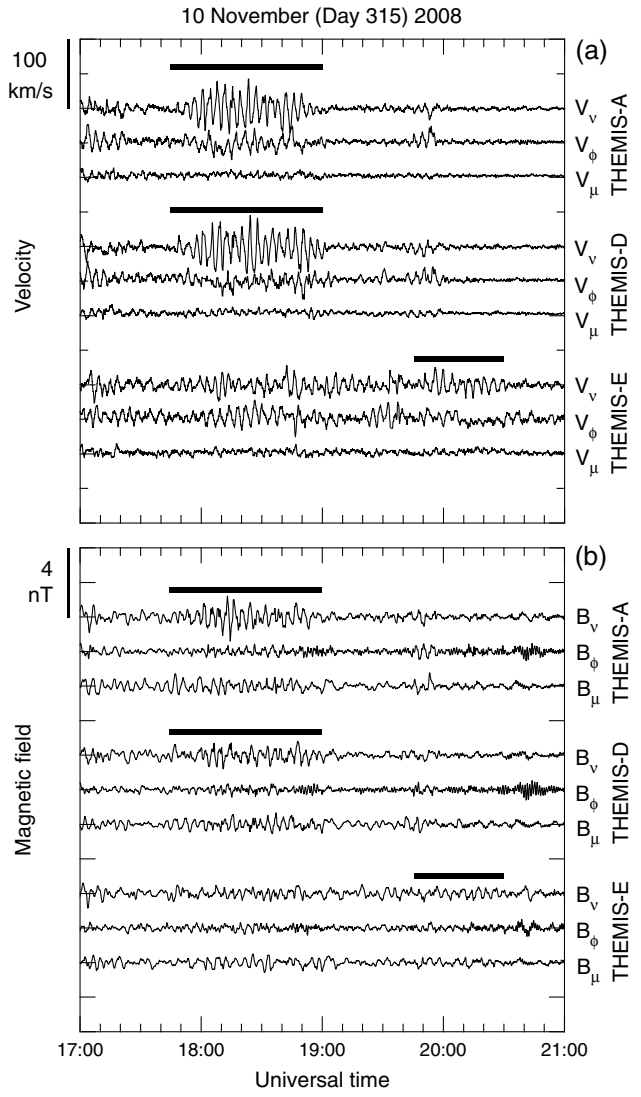

Figure 6. Ion bulk velocity and magnetic field for a 4 h interval on 10 November 2008 during which poloidal waves are detected by THEMIS spacecraft. (a) Ion bulk velocity at THEMIS-A, THEMIS-D, and THEMIS-E. The data are smoothed by 7 point (~21 s) running averages. Horizontal bars indicate intervals of poloidal oscillations: 1745–1900 UT at THEMIS-A and THEMIS-D and 1945–2030 UT at THEMIS-E. (b) Magnetic field at the same THEMIS spacecraft. The data are smoothed by 7 point (~21 s) running averages. In addition, slow variations are removed by subtracting 101 point (~303 s) running averages.

wave activity was limited to a small domain in the L versus magnetic local time (MLT) space centered at L ~11 and MLT ~ 0900. At GOES 11 ($L \sim 7$), the wave activity occurred also at ~0900 MLT.

[21] Included in Figure 4a are the model magnetopause by *Shue et al*. [1998] and the model bow shock by *Fairfield* [1971]. As input to the *Shue et al*. [1998] magnetopause model, we used the maximum solar wind dynamic pressure 0.7 Pa and the minimum B_z −2 nT during the selected 4 h interval (Figure 1). These values give an estimate of the smallest magnetopause standoff distance during the 4 h interval. According to the model, THEMIS-A, THEMIS-D, and THEMIS-E were approximately 2 R_E Earthward of the magnetopause. Therefore, we argue that our poloidal waves do not belong to the class of ULF waves reported by *Plaschke et al*. [2009], which are localized to the magnetopause.

[22] Figures 4b, 4c, and 4d show dipole-based magnetic coordinates of the four spacecraft as a function of time. As in Figure 4a, the thick line segments indicate poloidal wave activity. Important features to be noted here are that during the wave observations, THEMIS-A and THEMIS-D had nearly identical L values (Figure 4b) and a finite separation in MLT (Figure 4d), and THEMIS-D was closer to the magnetic equator than THEMIS-A (Figure 4c). GOES-11 was in the northern magnetosphere at a magnetic latitude (MLAT) of ~5°.

4. THEMIS Data

4.1. Bulk Velocity Dynamic Spectra

[23] The poloidal waves discussed in this paper were identified by visually surveying dynamic spectra of V, displayed in the format of Figure 5. The figure shows dynamic spectra for THEMIS-A, THEMIS-D, and THEMIS-E computed for the whole day of 10 November 2008. For each spacecraft, Figures 5a–5c show, from top to bottom, the power spectral density (PSD) of V_ν, the PSD of V_ϕ, and the V_ν-to-V_ϕ PSD ratio. The PSD is first calculated from the Fourier transform of the time series (described in section 2) in the positive frequency domain. This PSD is then multiplied by a factor of 2 to account for the power coming from the negative frequency [e.g., *Brautigam et al*., 2005]. The satellite position is given at the bottom using dipole-based coordinates.

[24] The V_ν and V_ϕ spectra at each THEMIS spacecraft exhibit continuous narrow-band enhancements at 3–5 mHz in the region outside of $L \sim 8$. In the daily dynamic spectra generated from the THEMIS-A data for the entire year of 2008, we find that this spectral feature is very common on the dayside. We attribute the narrow-band oscillations to fundamental standing Alfvén waves on the basis of previous satellite studies [e.g., *Singer and Kivelson*, 1979; *Anderson et al*., 1990; *Takahashi et al*., 2002] and also on the basis of comparison of the measured **V** and **B** oscillations at the THEMIS spacecraft. The waves are classified as toroidal waves, because they usually exhibit higher power in the V_ϕ component. In the example shown here, the dominance of toroidal waves is evident in the bottom panel because the V_ν-to-V_ϕ PSD ratio appears in blue in the 3–5 mHz band.

[25] For a short-time period ~1800–1900 UT, however, the PSD at THEMIS-A and THEMIS-D is higher in the V_ν component, indicating that the polarization of the Alfvén waves switched from toroidal to poloidal. In the bottom panel for each spacecraft, the vertical structure in red occupies a wide frequency band, but the top panel indicates that the wave power is concentrated in a narrow band around 4 mHz (period ~6 min, Pc5 band), similar to the toroidal waves that preceded the poloidal waves. A similar poloidal wave signature is seen at THEMIS-E when it was at ~0900 MLT. At this spacecraft, the occurrence of the wave is delayed by ~2 h relative to THEMIS-A and THEMIS-D, and the spectral intensity is lower.

4.2. Waveform

[26] Figure 6 presents time series plots of all components of the **V** and **B** vectors at the THEMIS spacecraft for

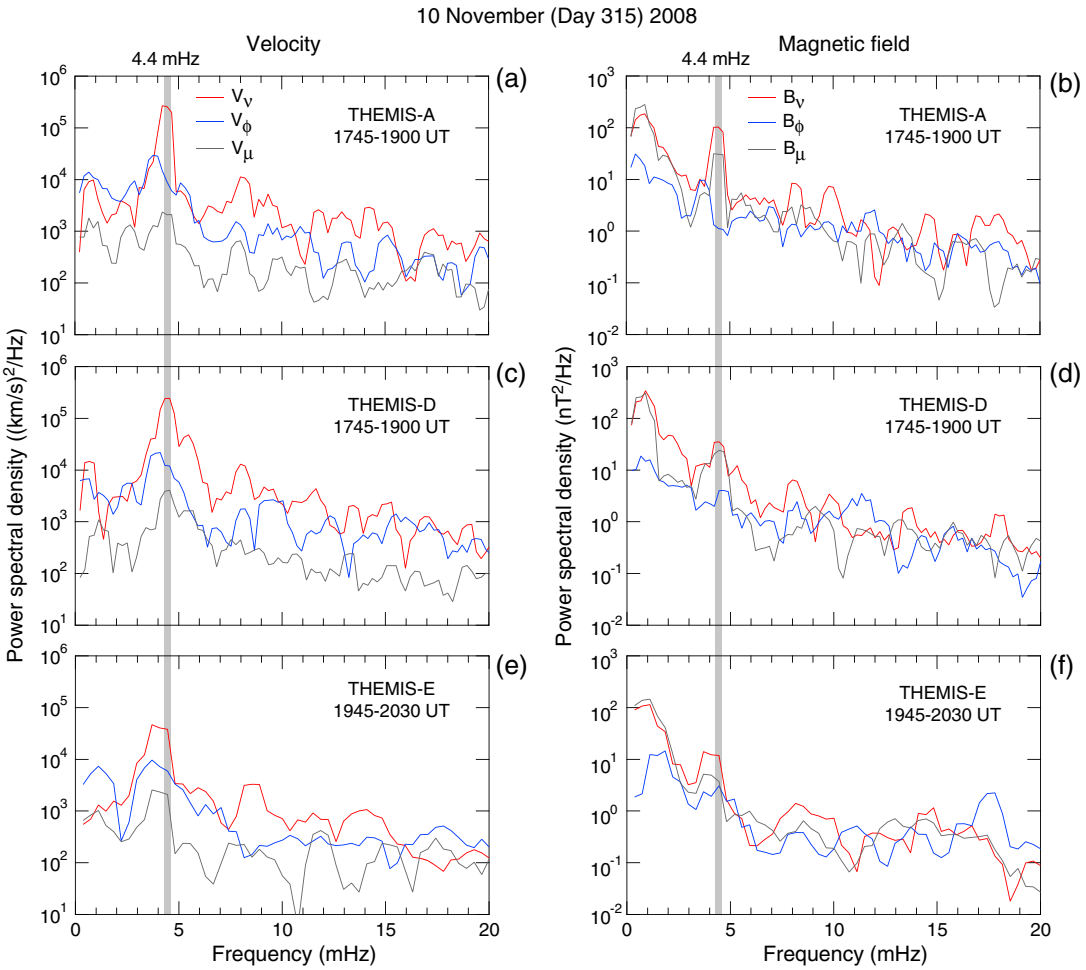

Figure 7. Power spectra of (a,c,e) ion bulk velocity and (b,d,f) magnetic field vector components computed for the time interval of poloidal waves at THEMIS-A, THEMIS-D, and THEMIS-E, as identified in Figures 5 and 6. The vertical lines indicate the frequency, 4.4 mHz, of the poloidal waves detected at THEMIS-A and THEMIS-D.

1700–2100 UT. To suppress random variations, both vectors have been smoothed by 7-point (~21 s) running averages. In addition, slow variations of **B** have been removed by subtracting 101 point (~303 s) running averages from the original 3 s time series. The heavy horizontal bars indicate intervals of poloidal waves: 1745–1900 UT at THEMIS-A and THEMIS-D and 1945–2030 UT at THEMIS-E.

[27] The poloidal waves at THEMIS-A and THEMIS-D exhibit very similar waveforms in both **V** and **B**. The maximum peak-to-peak amplitude of V_ν is 70 km/s, roughly 2 to 3 times larger than that of V_ϕ. The amplitude of V_μ is very small. Assuming that the electric field **E** is given by $\mathbf{E} = -\mathbf{V} \times \mathbf{B}$ and using the observed **B** with a magnitude of ~40 nT (data not shown), we estimate the peak-to-peak amplitude of the azimuthal component of the electric field to be ~3 mV/m. This amplitude is comparable to more commonly observed Pc5-band waves at THEMIS in the outer magnetosphere [*Sarris et al.*, 2009] but is much larger than the amplitude 0.2–0.5 mV/m of toroidal waves observed at geosynchronous orbit [*Junginger et al.*, 1984]. The peak-to-peak amplitude of the radial displacement of the magnetic field line is estimated to be ~4000 km.

[28] The magnetic field also exhibits a much larger oscillation in the radial (B_ν) component than in the azimuthal (B_ϕ) component. At THEMIS-A, the maximum peak-to-peak amplitude of B_ν is ~2 nT, which is ~5% of the background magnetic field (~40 nT). At THEMIS-D, the maximum peak-to-peak amplitude is ~1 nT. The higher B_ν amplitude at the spacecraft at larger distance from the magnetic equator (THEMIS-A, see Figure 4c) is consistent with odd-mode standing waves (see Figure 1). There is also a substantial compressional (B_μ) component in the **B** field oscillations, which is expected for waves excited in finite-β plasmas.

[29] The poloidal waves at THEMIS-E were observed with ~2 h delay from those at THEMIS-A and THEMIS-D. This delay is comparable to the orbital time delay (the universal time difference of the perigee passage) between the two spacecraft, which implies that the poloidal waves lasted long but were highly localized in local time. An alternative explanation is that the waves occupied a large MLT domain but were short lived; they were activated twice, first at ~1800 UT and then at ~2000 UT.

4.3. Power Spectrum

[30] Figure 7 shows the power spectra of the **V** and **B** vector components computed for the poloidal waves

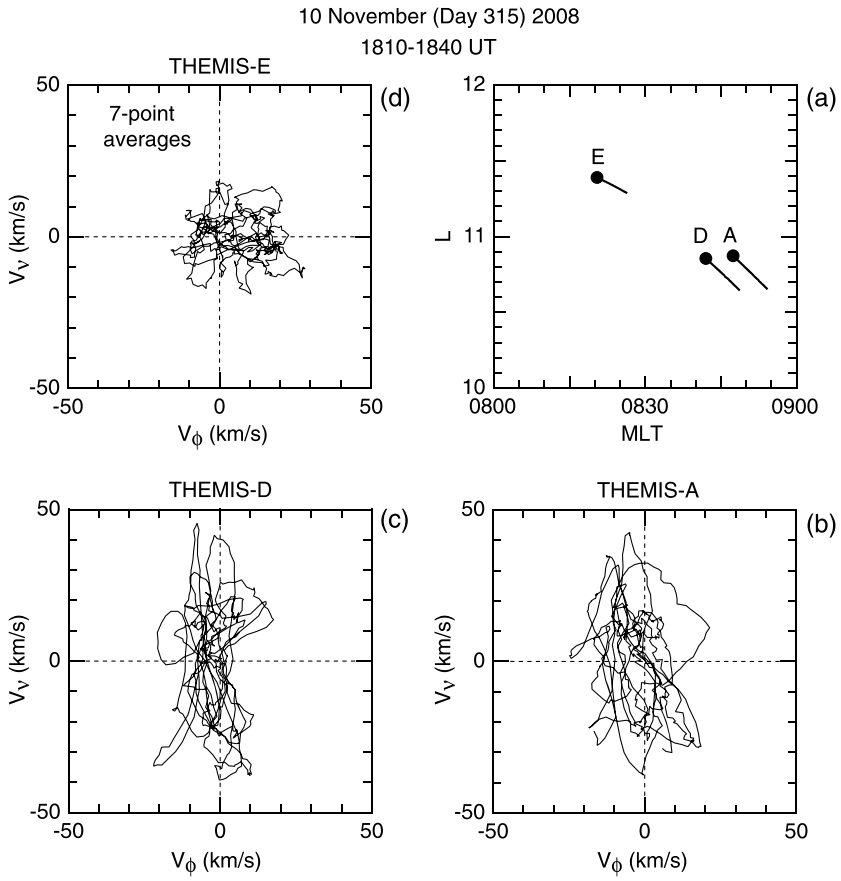

Figure 8. Hodographs showing the ion bulk velocity perturbations in the $\phi - v$ plane at three THEMIS spacecraft. Seven-point (~21 s) running averages of the original 3 s data are used for the hodographs. (a) L versus MLT location of THEMIS-A, THEMIS-D, and THEMIS-E for 1810–1840 UT on 10 November (day 315) 2008. The dot for each spacecraft indicates the position at 1810 UT. (b) Hodograph for THEMIS-A. (c) Hodograph for THEMIS-D. (d) Hodograph for THEMIS-E.

identified in Figure 6. Vertical lines are drawn at 4.4 mHz, the location of the highest V_v spectral peak at THEMIS-A and THEMIS-D. Spectral peaks at THEMIS-D occur at a slightly lower frequency, 4.0 mHz.

[31] In the velocity spectra (Figures 7a, 7c, and 7e), the V_v component exhibits the highest power in the band occupied by the poloidal waves, as expected. The second highest is the V_ϕ component, but its peak occurs at a lower frequency. This means that toroidal and poloidal waves coexisted but were not coupled. Uncoupled fundamental poloidal and toroidal modes can have different frequencies if their m numbers differ according to theoretical models [e.g., *Cummings et al*., 1969; *Ozeke and Mann*, 2005]. However, the models indicate that the fundamental poloidal mode has a lower frequency than the fundamental toroidal mode if excited on the same field line, opposite to our observations. Possible reasons for the higher poloidal frequency include excitation of the modes on slightly different L shells, Doppler shift of the high-m poloidal waves, and a finite pressure effect on the poloidal mode frequency. Finally, the V_μ component exhibits a peak at the frequency of the V_v spectral peak, but the V_μ power is 1.5 to 2 orders of magnitude lower than the V_v power.

[32] In the magnetic field spectra (Figures 7b, 7d, and 7f), the radial component B_v exhibits the highest spectral peak, at the frequency of the V_v spectral peak. This confirms that the designation of poloidal mode is appropriate from the magnetic field point of view also. Unlike the velocity spectra, however, the magnetic field spectra exhibit substantial power in the component along the ambient magnetic field, B_μ. The B_v/B_μ power ratio is 1.5 at THEMIS-D (MLAT ~ −2°), whereas the ratio is 3.3 at THEMIS-A (MLAT ~ −7°). The higher B_v/B_μ power ratio at the spacecraft farther away from the magnetic equator is consistent with the model of the fundamental standing wave illustrated in Figure 1a. According to that model, the ratio is an increasing function of |MLAT| because the B_v component of the fundamental mode has a node at the equator where field line tilt is zero, and because the B_μ component has an antinode at the equator where field line displacement is maximum. Qualitatively the same |MLAT| dependence of the B_v/B_μ power ratio was obtained for the Pg-related poloidal waves reported by *Takahashi et al*. [2011]. Note that the latitude dependence of wave amplitude near the magnetic equator alone cannot eliminate the possibility that the waves are the third or fifth harmonic instead of the fundamental.

[33] There is another interesting feature that the poloidal waves share with Pg waves. In Figure 7, both V_v and B_v exhibit a spectral peak at the second and possibly the third harmonics of the frequency of the main peak, which is located at ~4 mHz. In the time series plots of these

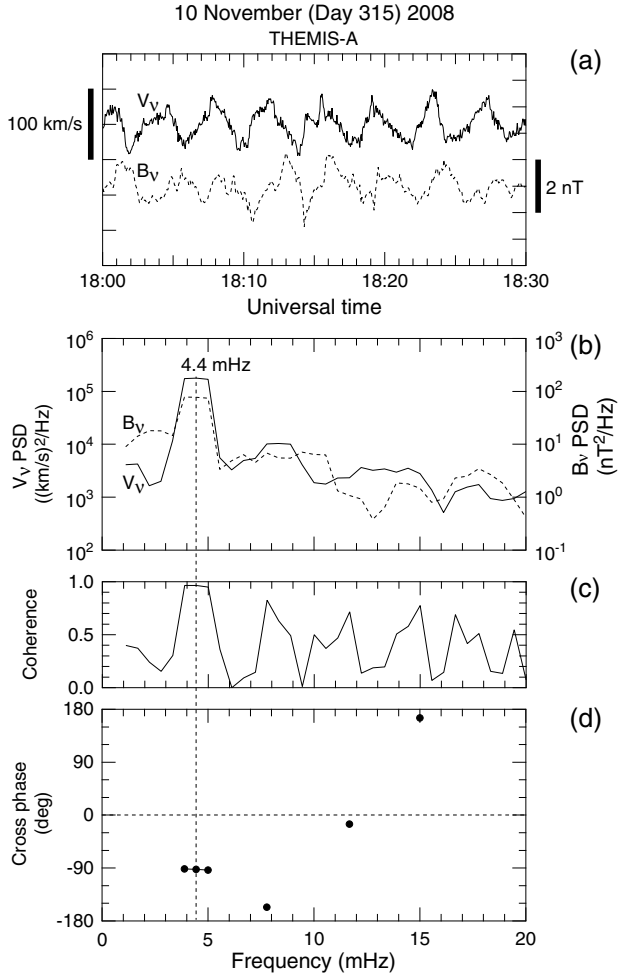

Figure 9. Comparison of the V_v and B_v components of the poloidal wave observed at THEMIS-A. (a) Time series. (b–d) Cross-spectral parameters computed with the number of degrees of freedom of 6. The cross phase is displayed only when coherence is higher than 0.7. The vertical dashed line indicates the center of the spectral peak of the poloidal wave.

components (shown later in Figure 9a), we find that the waveform is not exactly sinusoidal with a tendency to be triangular. This waveform distortion explains the higher harmonics in the spectra. A similar behavior was found in the B_μ component observed near the magnetic equator during the Pg event reported by *Takahashi et al*. [2011, Figure 10]. We speculate that the same mechanism is causing the waveform distortion. Also, we note that equatorially confined waveform distortion (called frequency doubling) occurs in the B_μ component during antisymmetric compressional Pc5 wave events [e.g., *Takahashi et al*., 1987] and that models have been proposed for this phenomenon [*Southwood and Kivelson*, 1997; *Mann et al*., 1999; *Sibeck et al*., 2012]. Testing whether any of these models can be used to explain the waveform distortion of the fundamental poloidal waves reported here is beyond the scope of this paper.

4.4. Velocity Hodograph

[34] Hodograph plots are helpful for intuitively understanding wave polarization and the spatial variation of wave properties. Figure 8 shows the V_v versus V_ϕ hodographs at the three THEMIS spacecraft for 1810–1840 UT, the center of the poloidal wave activity observed by THEMIS-A and THEMIS-D. The tracks of the spacecraft in the L versus MLT plane are shown in Figure 8a. THEMIS-A and THEMIS-D had virtually identical L values as they moved inward but were separated in MLT.

[35] The hodographs at THEMIS-A (Figure 8b) and THEMIS-D (Figure 8c) are highly elongated in the radial direction and have comparable amplitudes. At THEMIS-E (Figure 8d), located just 0.6 R_E outward in the radial direction and 0.5 h earlier in MLT, the V_v amplitude is small and the hodograph does not show radial elongation. This observation implies that the poloidal waves at THEMIS-A and THEMIS-D were not directly driven by sources located in the solar wind (i.e., solar wind pressure pulses) or on the magnetopause (i.e., the Kelvin-Helmholtz instability).

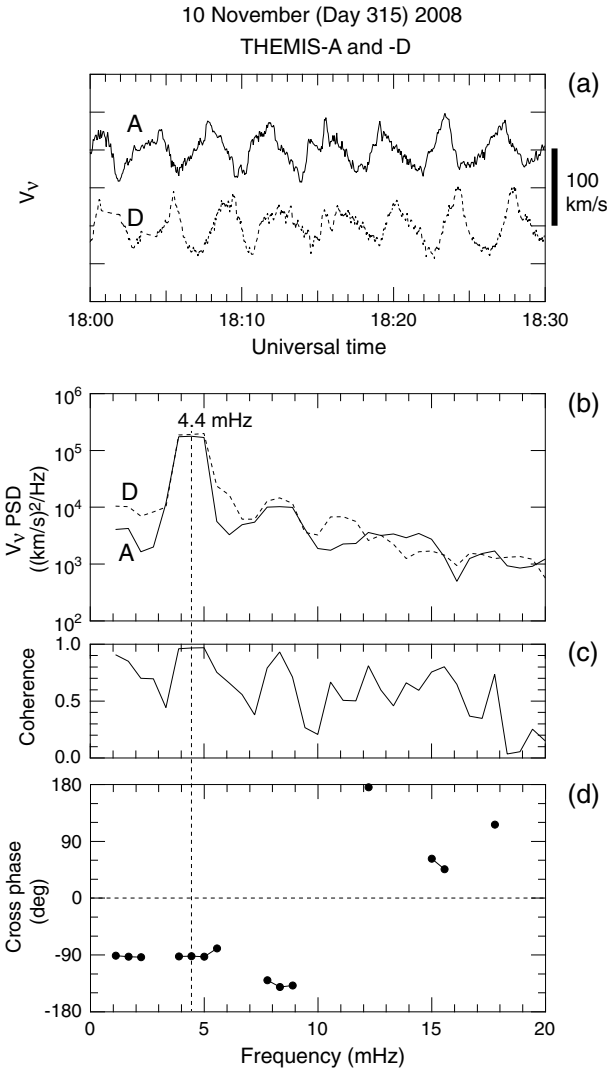

Figure 10. Phase delay analysis of the poloidal waves observed by THEMIS-A and THEMIS-D. (a) Comparison of the V_v waveforms at the two spacecraft. (b–d) Results of cross-spectral analysis of the V_v oscillations shown in Figure 10a.

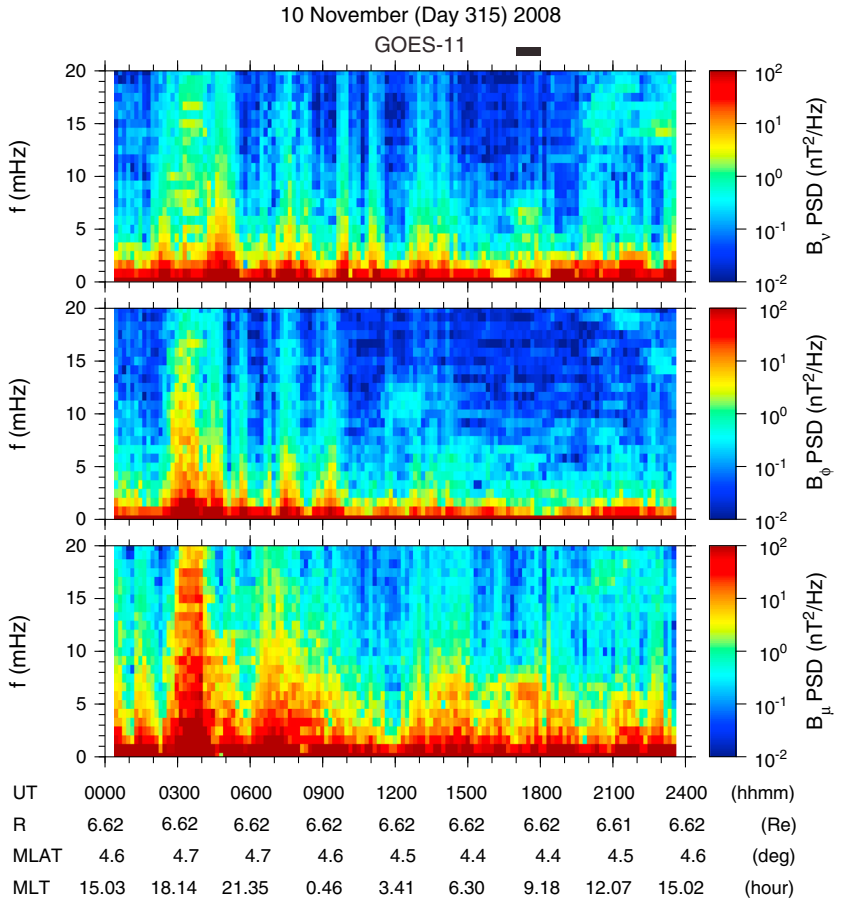

Figure 11. Dynamic spectra of the magnetic field data from the GOES-11 geostationary spacecraft for 10 November 2008. The horizontal bar at the top indicates poloidal wave.

4.5. Phase Delay Between Velocity and Magnetic Field

[36] We can determine the standing wave mode of the poloidal waves by examining the phase delay between oscillations in the velocity and magnetic field. Figure 9a shows V_v and B_v data from THEMIS-A for a 30 min period during the poloidal wave event. From visual examination of the plots, it is obvious that the peaks of B_v lag behind the peaks of V_v by a fraction of the wave period. Spectral analysis of the time series yields spectral peaks centered at the identical frequency of 4.4 mHz (Figure 9b), high coherence at this frequency (Figure 9b), and a cross phase of −90° (the B_v phase is delayed from the V_v phase by 90°). The cross phase is exactly what we expect for a fundamental poloidal wave observed south of the magnetic equator, as illustrated in Figure 1a.

4.6. Azimuthal Wave Number

[37] The relative position of the THEMIS-A and THEMIS-D, shown in Figures 4 and 8, allows us to determine the azimuthal wave number of the poloidal waves by cross spectral analysis. Figure 10 shows the results obtained for 1800–1830 UT. At the midpoint of this time interval, the two spacecraft were separated by 0.02 R_E in the radial (L) direction and by 0.25 R_E in the azimuthal (MLT) direction. Therefore, it is reasonable to attribute the phase delay between the spacecraft to azimuthal propagation of the waves. In Figure 10a, it is obvious that the two spacecraft detected very similar V_v oscillations but with a finite time delay. The spectral analysis of the time series indicates that the V_v oscillations had an identical frequency of 4.4 mHz (Figure 10b), high coherence at this frequency (Figure 10c), and a cross phase value of −92° (THEMIS-D lagged behind THEMIS-A by 92°) (Figure 10d). Because $2n\pi$ ambiguity is intrinsic in two-point phase delay measurement, we consider another possibility. By adding 2π (360°) to the nominal −92° phase delay, we get a phase delay of 268°.

[38] We have estimated the wave properties for each of the two cross phase values as follows. If the cross phase value is −92°, the waves propagated westward (or tailward) at a speed of ~30 km/s, had an azimuthal wave number of approximately −70, and had an azimuthal wavelength of ~6000 km. The corresponding ionospheric attenuation factor (equation (2)) is found to be ~10^{-2}. If the cross phase value is 268°, the waves propagated eastward (or sunward) at a velocity of ~10 km/s, had an azimuthal wave number of ~200, and had an azimuthal wavelength of ~2000 km. The ionospheric attenuation factor is found to be ~10^{-6}. In either case, the $|m|$ value was too large for the waves to reach the ground through the ionosphere [*Hughes and Southwood*, 1976]. We will confirm this prediction in section 6.

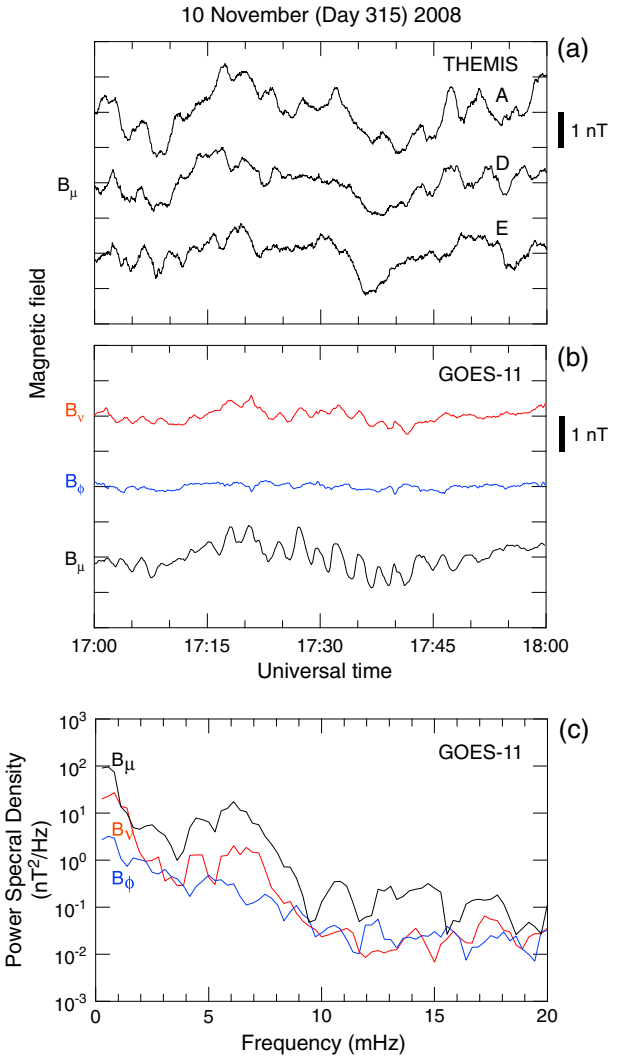

Figure 12. Multisatellite magnetic field data for the time period of compressional poloidal waves at GOES-11. (a) B_μ-component time series at the THEMIS-A, THEMIS-D, and THEMIS-E spacecraft. (b) Three components of the magnetic field at GOES-11. (c) Power spectra of the GOES-11 magnetic field data shown in Figure 12b.

5. GOES-11 Data

5.1. Dynamic Spectra

[39] Compressional magnetic field oscillations possibly related to the poloidal waves at the THEMIS spacecraft were observed at GOES-11. As shown in Figure 4, GOES-11 was located in the same local time sector as THEMIS-A and THEMIS-D but approximately 2 R_E inward. Figure 11 shows dynamic spectra of the GOES-11 magnetic field for 10 November 2008. The compressional oscillations appear between 1700 and 1800 UT (a horizontal bar at the top indicates this time period) at ~6 mHz as an enhancement in the B_μ spectra. This spectral enhancement accompanies a similar but weaker spectral feature in the B_v component. The universal time of the wave activity at GOES-11 is ~1 h earlier than that at THEMIS-A and THEMIS-D, but the local times match well (see Figure 4).

5.2. Waveform and Power Spectrum

[40] Figure 12 compares magnetic field data from the THEMIS and GOES spacecraft for 1700–1800 UT, during which GOES-11 detected compressional waves. For this period, GOES-11 was located at the thick portion of the orbit trace shown in Figure 4, and the THEMIS spacecraft were close to their apogees. The spacecraft were all located at ~0900 MLT. The B_μ components at the THEMIS spacecraft (Figure 12a) are all similar, exhibiting oscillations with both long (~30 min) and short (~5 min) periods. The overall similarity among the three spacecraft implies that much of the variations originated from solar wind sources, such as changes in the solar wind dynamic pressure. Disturbances or upstream waves associated with quasi-parallel shock are unlikely to be the cause of the oscillations because the IMF cone angle was large (Figure 2h). The B_v and B_μ components at GOES-11 (Figure 12b) also show slow (~30 min) oscillations, with waveform similar to that at THEMIS. By contrast, the regular 3 min oscillations seen at GOES-11 at 1715–1750 UT in the B_v and B_μ components are not seen at THEMIS. The power spectra (Figure 12c) of the GOES-11 magnetic field for the 1 h interval show a spectral peak in the B_μ and B_v components at 6 mHz. The B_v-to-B_μ power ratio at the peak is 0.12, corresponding to a B_v-to-B_μ amplitude ratio of 0.34.

[41] The 6 mHz waves at GOES-11 have similarities to the previously reported poloidal waves that were associated with Pgs. During Pg events observed on the ground, spacecraft located at magnetic latitudes below ~5° observe compressional ($B_\mu > B_v$, B_ϕ) oscillations with amplitude on the order of 1 nT [*Kokubun*, 1980; *Hillebrand et al.*, 1982; *Kokubun et al.*, 1989; *Takahashi et al.*, 1992; *Takahashi et al.*, 2011]. The compressional oscillations are attributed to fundamental poloidal waves. The B_v-to-B_μ amplitude ratio increases with magnetic latitude, which is consistent with field line displacement associated with the fundamental mode.

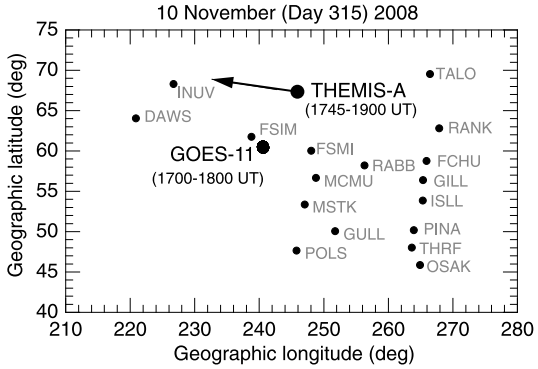

Figure 13. Northern foot points of THEMIS-A for 1800–1900 UT and GOES-11 for 1700–1800 UT on 2008 day 315, shown in geographic coordinates. The foot points were given using the combined IGRF and T89c magnetic field models for each 1 h interval. The small solid circles indicate the location of CARISMA and THEMIS GBO magnetometers from which data are available for the time interval of the ULF waves observed from the spacecraft.

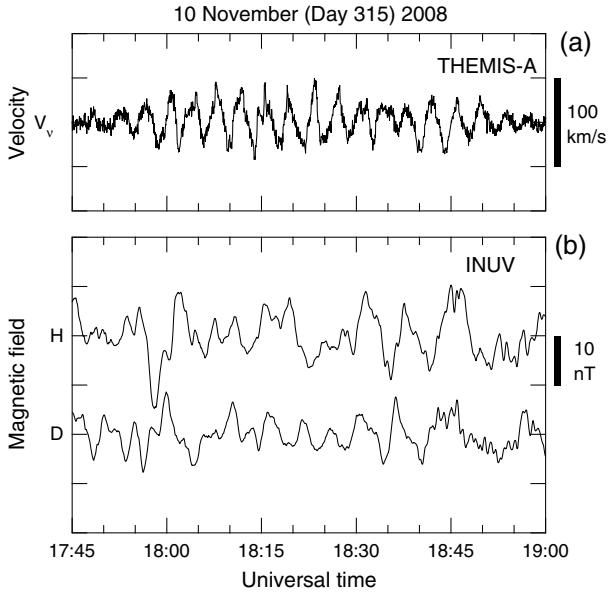

Figure 14. (a) V_v component at THEMIS-A during the poloidal wave event. (b) Magnetic field H (northward) and D (eastward) components at the Inuvik (INUV) station, which was near the magnetic field foot point of THEMIS-A. Ten-minute running averages have been removed from the data.

6. Ground Magnetic Field Data

[42] Alfvén waves propagate along the field line to the ionosphere, but whether or not they reach the ground depends on the wavelength in the plane of the ionosphere, as mentioned in section 1.3. We examined magnetic field data from stations near the magnetic field foot points of the spacecraft to determine whether the poloidal waves propagated to the ground. Figure 13 shows the location of the CARISMA and THEMIS-GBO magnetometers that were in operation at the time of the poloidal wave event. The track with an arrowhead indicates the magnetic field foot point of THEMIS-A for 1800–1900 UT calculated using the combined IGRF and T89c models. The IOPT input parameter, which is an integer in the range from 1 to 7, required for the T89c model was set equal to 1 considering the low geomagnetic activity, $Kp < 1$. The large filled circle is the GOES-11 foot point for 1700–1800 UT. We examined data from all stations in the map, but only show data from the stations closest to the spacecraft foot points.

[43] Figure 14 compares the V_v component at THEMIS-A (Figure 14a) and the northward (H) and eastward (D) components of the magnetic field at the Inuvik (INUV) station (Figure 14b). Oscillations are present at both locations, but they are not the same. At THEMIS-A, the velocity oscillation is very regular although it is amplitude modulated and consists of two wave packets. On the ground, the oscillation is very irregular with comparable amplitudes in H and D. We do not see any wave packet structure in the ground data resembling that at THEMIS-A.

[44] Figure 15 compares the compressional magnetic field oscillation at GOES-11 with magnetic field variations in the X (northward) and Y (eastward) components at Fort Simpson (FSIM) and Fort Smith (FSMI). Here again, we do not see any evidence that the B_μ oscillation (Figure 15a) propagated to the ground (Figure 15b). The implication is that the compressional poloidal waves at GOES-11 had a large azimuthal wave number similar to that at THEMIS.

7. Discussion

7.1. Summary of the Observations

[45] We can summarize the above observations of fundamental poloidal waves as follows.

[46] 1. The waves were observed when the geomagnetic activity was low.

[47] 2. The poloidal nature of the waves is evident in the strong radial perturbations of the ion bulk velocity and the magnetic field.

[48] 3. The waves were observed by three THEMIS spacecraft in the prenoon sector (MLT ~ 0900) of the outer ($L \sim 11$) magnetosphere. GOES-11, located in the same local time sector but at $L \sim 7$, also observed waves with magnetic field polarization consistent with that at THEMIS.

[49] 4. The poloidal waves exhibited strong evidence of a fundamental mode structure along the background magnetic field. The evidence includes: similarity of the frequency (~4 mHz at THEMIS) to the frequency of fundamental toroidal waves documented in section 4.3; large velocity perturbations and small transverse magnetic field perturbations near the equator; and phase delay between velocity and magnetic field that matches the theoretical prediction.

[50] 5. The poloidal waves had an azimuthal wave number of large magnitude, either approximately −70 (westward propagation) or ~200 (eastward propagation). The corresponding azimuthal phase velocity was either ~30 km/s or ~7 km/s, and azimuthal wavelength was either ~6000 km or ~2000 km.

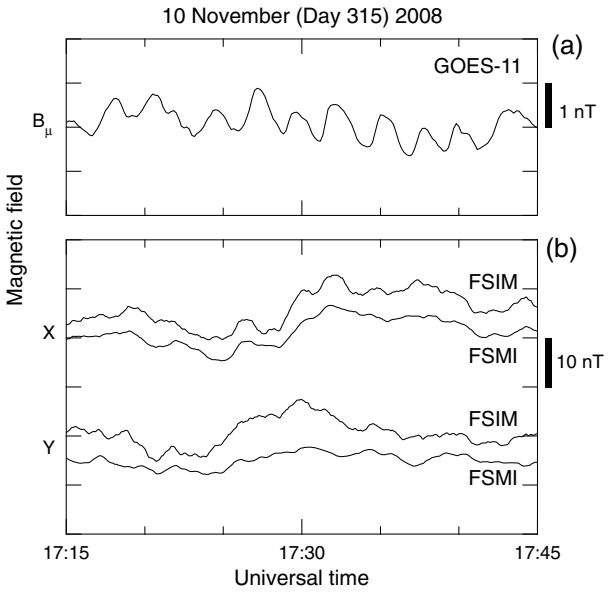

Figure 15. (a) B_μ component at GOES-11 during the poloidal wave event. (b) Magnetic field X (northward) and Y (eastward) components on the ground at Fort Simpson (FSIM) and Fort Smith (FSMI), which were close to the magnetic field foot point of GOES-11.

[51] 6. Near the foot points of the spacecraft, there were no monochromatic magnetic field pulsations corresponding to the poloidal waves. This result is consistent with the large $|m|$ value of the poloidal waves for which ionospheric screening is very effective.

7.2. Theoretical Model of the Fundamental Poloidal Mode

[52] To confirm that the observed poloidal waves were excited at the fundamental mode, we estimated the frequency and amplitudes of the mode using a theoretical model. To compare with the THEMIS-A observations at ~1815 UT, we selected a dipole field line at $L = 10.8$, specified the mass density (ρ) variation along the field line using a simple model $\rho = \rho_{eq}(LR_E/R)^1$ [e.g., *Denton et al*., 2006], and numerically solved the poloidal wave equation [*Cummings et al*., 1969]. Here ρ_{eq} is the equatorial mass density and R is geocentric distance to the field line. The value of ρ_{eq} was chosen to be 0.5 amu.cm^{-3} from the ion moments calculated from the ESA data. We assumed all-hydrogen plasma, which is appropriate for 2008, because heavy ions make little contribution to the mass density near the solar minimum [*Denton et al*., 2011].

[53] The theoretical frequency for the fundamental poloidal wave is 2.5 mHz. This is lower than the observed frequency 4.4 mHz. However, the discrepancy is reduced when we note that the dipole field at the equator (23 nT) is weaker than the measured field (40 nT). A stronger magnetic field means a higher Alfvén velocity ($\propto B/\sqrt{\rho}$) and thus a higher standing wave frequency. The equatorial Alfvén velocity, the lowest along a field line, largely determines the frequency of standing Alfvén waves. Therefore, for a better estimate of the mode frequency, we multiply the theoretical frequency by the magnetic field ratio (=40/23) and obtain a corrected theoretical frequency of 4.3 mHz. This last frequency is very close to the observed frequency.

[54] We used the same dipole calculation to estimate the B_r (nT)-to-E_ϕ (mV/m) amplitude ratio for the fundamental poloidal mode. The theoretical ratio, evaluated at the magnetic latitude of −7°, the location of THEMIS-A at the middle of the wave event, is 0.24. This is substantially lower than the ratio ~0.7 obtained from the B_r amplitude of ~2 nT and the E_ϕ amplitude of ~3 mV/m described in section 4.2. However, this discrepancy can also be attributed to the dipole field being weaker than the measured magnetic field. For Alfvén waves, the phase velocity is proportional to the **E**-to-**B** amplitude ratio, so the ratio from the dipole calculation should be multiplied by the same factor (40/23) to be compared with the observation. After this correction, the theoretical ratio becomes ~0.4, which is closer to the observational ratio. Possible contributing factors to the remaining discrepancy include a slight shift of the B_r node from the magnetic equator and inaccuracy of the model for the field line mass distribution.

7.3. Possible Generation Mechanisms

[55] We briefly discuss possible excitation mechanisms of the observed poloidal waves based on the ion and electron moments derived from the ESA data. During the poloidal wave event at THEMIS-A, we find that the plasma density was ~0.5 cm^{-3}, the ion and electron temperatures were both ~1 keV, and the corresponding value of the plasma β was ~0.2.

[56] When the β value is low (<1), energetic particles can excite Alfvén waves through drift-bounce resonance [e.g., *Southwood*, 1976]. For example, studies of Pgs [*Thompson and Kivelson*, 2001; *Takahashi et al*., 2011] suggested that fundamental poloidal waves are driven by ring current ions through the drift resonance

$$\omega - m\omega_d = 0. \tag{3}$$

[57] This is a special case, $N = 0$, of the general drift-bounce resonance given in equation (1). Because the magnetic field gradient and curvature drift of ions is westward, the m number must be negative (westward-propagating wave) for this resonance to occur. This is indeed the case for Pgs [e.g., *Poulter et al*., 1983].

[58] The same resonance is possible for the poloidal waves studied here. Adopting $m \sim -70$, one of the options for m described in section 4.6 and using the guiding center velocity for the dipole magnetic field [*Hamlin et al*., 1961], we find that the ion resonance energy is ~15 keV.

[59] However, this is not the only possibility. During the wave event, which was observed at $L \sim 11$, the electron temperature was about the same as the ion temperature, which means that the particle energy density was about the same for the two species. Therefore, it is also possible that electrons contributed to wave excitation. This situation is different from $L \sim 6$, the location of Pgs, where the energy density is generally higher for ions [*Daglis et al*., 1999]. Noting that the electron drift is eastward, we adopt the other option described in section 4.6, $m \sim 200$ (eastward-propagating wave), and find that the electron resonance energy is ~5 keV, not too far from the electron thermal energy.

[60] The drift resonance condition only describes the channel through which energy is exchanged between waves and particles. Whether or not waves are excited by the resonant particles depends on the availability of particle free energy. A possible free energy for fundamental poloidal waves, previously discussed for Pgs, is an inward gradient of the ion phase space density that is steeper than the gradient of ions with the first two adiabatic invariants, μ (not to be confused with the coordinate axis along the magnetic field) and J, conserved [*Southwood*, 1976; *Chen and Hasegawa*, 1991]. The formation of such a gradient would imply processes to violate μ or J, so higher frequency waves are probably involved. We plan to conduct an analysis of the phase space density in a separate study.

[61] Another mechanism suggested for fundamental poloidal waves is the drift wave instability of the compressional Alfvén wave [*Hasegawa*, 1971; *Green*, 1979, 1985]. Because this instability requires high concentration of cold plasma (the plasmasphere), it is not likely that the mechanism was responsible for the poloidal waves observed by THEMIS at $L \sim 11$.

8. Conclusions

[62] In conclusion, we have presented multispacecraft observations of fundamental poloidal waves in the prenoon sector of the outer magnetosphere. By examining ion bulk velocity and magnetic field data from three THEMIS spacecraft, we concluded that the poloidal mode had a fundamental

(odd mode) standing wave structure along the background magnetic field. Furthermore, using data from a pair of THEMIS spacecraft that had a separation vector in the azimuthal direction, we were able to determine the azimuthal phase delay and possible values of the azimuthal wave number. The wave number was such that the ionosphere screening effect renders the waves undetectable on the ground. Although the present study is limited to waves observed on a single day, it nevertheless demonstrates that fundamental poloidal waves occur in the magnetosphere without clearly associated ground magnetic pulsations (e.g., Pgs). A systematic event survey is required to establish the spatial occurrence pattern of fundamental poloidal waves and the factor controlling their occurrence. Also, the particle distribution function associated with the poloidal waves need to be examined to identify the generation mechanism of the waves.

[63] **Acknowledgments.** The authors thank I. R. Mann, D. K. Milling, and the rest of the CARISMA team for data used in Figure 15. CARISMA is operated by the University of Alberta and funded by the Canadian Space Agency. The work by KT was financially supported by NASA grants NNX10AK93G and NNX13AE02G. The work by MDH was financially supported by the National Science Foundation under Award AGS-1230398. The work by K-HG was financially supported by the German Ministerium für Wirtschaft und Technologie and the Deutsches Zentrum für Luft und Raumfahrt under grant 50QP0402.

[64] Robert Lysak thanks Mark Engebretson and Louis Ozeke for their assistance in evaluating this paper.

References

Anderson, B. J., M. J. Engebretson, S. P. Rounds, L. J. Zanetti, and T. A. Potemra (1990), A statistical study of Pc3-5 pulsations observed by the AMPTE/CCE magnetic field experiment, 1, Occurrence distributions, *J. Geophys. Res.*, *95*(A7), 10,495–10,523.

Angelopoulos, V. (2008), The THEMIS mission, *Space Sci. Rev.*, *141*, 5–34, doi:10.1007/s11214-008-9336-1.

Arthur, C. W., and R. L. McPherron (1981), The statistical character of Pc4 magnetic pulsations at synchronous orbit, *J. Geophys. Res.*, *86*(A3), 1325–1334.

Auster, H. U., et al. (2008), The THEMIS fluxgate magnetometer, *Space Sci. Rev.*, *141*, 235–264, doi:10.1007/s11214-008-9365-9.

Baddeley, L. J., T. K. Yeoman, D. M. Wright, K. J. Trattner, and B. J. Kellet (2004), A statistical study of unstable particle populations in the global ring current and their relation to the generation of high *m* ULF waves, *Ann. Geophys.*, *22*, 4229–4241.

Baddeley, L. J., T. K. Yeoman, and D. M. Wright (2005), HF Doppler sounder measurements of the ionospheric signatures of small scale ULF waves, *Ann. Geophys.*, *23*(5), 1807–1820.

Bendat, J. S., and A. G. Piersol (1971), *Random Data: Analysis and Measurement Procedures*, p. 407, John Wiley, New York.

Bonnell, J. W., F. S. Mozer, G. T. Delory, A. J. Hull, R. E. Ergun, C. M. Cully, V. Angelopoulos, and P. R. Harvey (2008), The electric field instrument (EFI) for THEMIS, *Space Sci. Rev.*, *141*, 303–341.

Brautigam, D. H., G. P. Ginet, J. M. Albert, J. R. Wygant, D. E. Rowland, A. Ling, and J. Bass (2005), CRRES electric field power spectra and radial diffusion coefficients, *J. Geophys. Res.*, *110*, A02214, doi:10.1029/2004JA010612.

Brekke, A., T. Feder, and S. Berger (1987), Pc4 giant pulsations recorded in Tromsø, 1929–1985, *J. Atmos. Terr. Phys.*, *49*(10), 1027–1032.

Chan, A. A., M. Xia, and L. Chen (1994), Anisotropic Alfven-ballooning modes in Earth's magnetosphere, *J. Geophys. Res.*, *99*(A9), 17,351–17,366.

Chen, L., and A. Hasegawa (1974), A theory of long-period magnetic pulsations, 1, Steady state excitation of field line resonance, *J. Geophys. Res.*, *79*(7), 1024–1032.

Chen, L., and A. Hasegawa (1991), Kinetic theory of geomagnetic pulsations, 1, Internal excitation by energetic particles, *J. Geophys. Res.*, *96*(A2), 1503–1512.

Cheng, C. Z., and Q. Qian (1994), Theory of ballooning-mirror instabilities for anisotropic pressure plasmas in the magnetosphere, *J. Geophys. Res.*, *99*(A6), 11,193–11,209.

Chisham, G. (1996), Giant pulsations: An explanation for their rarity and occurrence during geomagnetically quiet times, *J. Geophys. Res.*, *101*(A11), 24,755–24,763.

Chisham, G., and D. Orr (1991), Statistical studies of giant pulsations (Pgs): Harmonic mode, *Planet. Space Sci.*, *39*(7), 999–1006, doi:10.1016/0032-0633(91)90105-J.

Cummings, W. D., R. J. O'Sullivan, and P. J. Coleman, Jr. (1969), Standing Alfvén waves in the magnetosphere, *J. Geophys. Res.*, *74*(3), 778–793.

Cummings, W. D., S. E. DeForest, and R. L. McPherron (1978), Measurements of the Poynting vector of standing hydromagnetic waves at geosynchronous orbit, *J. Geophys. Res.*, *83*(A2), 697–706, doi:10.1029/JA083iA02p00697.

Daglis, I. A., R. M. Thorne, W. Baumjohann, and S. Orsini (1999), The terrestrial ring current: Origin, formation, and decay, *Rev. Geophys.*, *37*(4), 407–438.

Denton, R. E., K. Takahashi, I. A. Galkin, P. A. Nsumei, X. Huang, B. W. Reinisch, R. R. Anderson, M. K. Sleeper, and W. J. Hughes (2006), Distribution of density along magnetospheric field lines, *J. Geophys. Res.*, *111*, A04213, doi:10.1029/2005JA011414.

Denton, R. E., M. F. Thomsen, K. Takahashi, R. R. Anderson, and H. J. Singer (2011), Solar cycle dependence of bulk ion composition at geosynchronous orbit, *J. Geophys. Res.*, *116*, A03212, doi:10.1029/2010JA016027.

Dungey, D. W. (1954), Electrodynamics of the outer atmosphere, *Pa. State Univ. Ionos. Res. Sci. Rept*, *69*.

Engebretson, M. J., L. J. Zanetti, T. A. Potemra, D. M. Klumpar, R. J. Strangeway, and M. H. Acua (1988), Observations of intense ULF pulsation activity near the geomagnetic equator during quiet times, *J. Geophys. Res.*, *93*(A11), 12,795–12,816.

Eriksson, P. T. I., L. G. Blomberg, A. D. M. Walker, and K.-H. Glassmeier (2005), Poloidal ULF oscillations in the dayside magnetosphere: A cluster study, *Ann. Geophys.*, *23*, 2679–2686.

Fairfield, D. H. (1971), Average and unusual locations for the earth's magnetopause and bow shock, *J. Geophys. Res.*, *76*, 6700–6716.

Glassmeier, K.-H. (1980), Magnetometer array observations of a giant pulsation event, *J. Geophys.*, *48*, 127–138.

Glassmeier, K.-H. (1984), On the influence of ionospheres with non-uniform conductivity distribution on hydromagnetic waves, *J. Geophys.*, *54*(2), 125–137.

Glassmeier, K. H., and M. Stellmacher (2000), Concerning the local time asymmetry of Pc5 wave power at the ground and field line resonance width, *J. Geophys. Res.*, *105*(A8), 18,874–18,855.

Glassmeier, K. H., S. Buchert, U. Motschmann, A. Korth, and A. Pederson (1999), Concerning the generation of geomagnetic giant pulsations by drift-bounce resonance ring current instabilities, *Ann. Geophys.*, *17*, 338–350.

Green, C. A. (1979), Observations of Pg pulsations in the Northern Auroral Zone and at lower latitude conjugate regions, *Planet. Space Sci.*, *27*, 63–77, doi:10.1016/0032-0633(79)90148-X.

Green, C. A. (1985), Giant pulsations in the plasmasphere, *Planet. Space Sci.*, *33*(10), 1155–1168, doi:10.1016/0032-0633(85)90073-X.

Haerendel, G., W. Baumjohann, E. Georgescu, R. Nakamura, L. M. Kistler, B. Klecker, H. Kucharek, A. Vaivads, T. Mukai, and S. Kokubun (1999), High-beta plasma blobs in the morningside plasma sheet, *Ann. Geophys.*, *17*, 1592–1601, doi:10.1007/s00585-999-1592-1.

Hamlin, D. A., R. Karplus, R. C. Vik, and K. M. Watson (1961), Mirror and azimuthal drift frequencies for geomagnetically trapped particles, *J. Geophys. Res.*, *66*(1), 1–4.

Hartinger, M. D., V. Angelopoulos, M. B. Moldwin, K. Takahashi, and L. B. N. Clausen (2013 accepted), Statistical study of global modes outside the plasmasphere, *J. Geophys. Res. Space Physics*, *118*, doi:10.1002/jgra.50140.

Hasegawa, A. (1971), Drift wave instability at the plasmapause, *J. Geophys. Res.*, *76*(22), 5361–5364.

Hillebrand, O., J. Münch, and R. K. McPherron (1982), Ground-satellite correlative study of a giant pulsation event, *J. Geophys.*, *51*, 129–140.

Hughes, W. J., and D. J. Southwood (1976), The screening of micropulsation signals by the atmosphere and ionosphere, *J. Geophys. Res.*, *81*, 3234–3247.

Hughes, W. J., D. J. Southwood, B. Mauk, R. L. McPherron, and J. N. Barfield (1978), Alfven waves generated by an inverted plasma energy distribution, *Nature*, *275*, 43–45.

Junginger, H., G. Geiger, G. Haerendel, F. Melzner, E. Amata, and B. Higel (1984), A statistical study of dayside magnetospheric electric field fluctuations with periods between 150 and 600 s, *J. Geophys. Res.*, *89*(A7), 5495–5505.

Kivelson, M. G., J. Etcheto, and J. G. Trotignon (1984), Global compressional oscillations of the terrestrial magnetosphere: The evidence and a model, *J. Geophys. Res.*, *89*(A11), 9851–9856.

Kokubun, S. (1980), Observations of Pc pulsations in the magnetosphere: Satellite-ground correlation, *J. Geomag. Geoelectr.*, *32*(SII), 17–39.

Kokubun, S., K. N. Erickson, T. A. Fritz, and R. L. McPherron (1989), Local time asymmetry of Pc 4-5 pulsations and associated particle modulations at synchronous orbit, *J. Geophys. Res.*, *94*(A6), 6607–6625.

Mann, I. R., G. Chisham, and J. A. Wanliss (1999), Frequency-doubled density perturbations driven by ULF pulsations, *J. Geophys. Res.*, *104*, 4559–4565, doi:10.1029/1998JA900136.

Mann, I. R., et al. (2008), The upgraded CARISMA magnetometer array in the THEMIS era, *Space Sci. Rev.*, *141*, 413–451.

McFadden, J. P., C. W. Carlson, D. Larson, J. Bonnell, F. Mozer, V. Angelopoulos, K.-H. Glassmeier, and U. Auster (2008), THEMIS ESA first science results and performance issues, *Space Sci. Rev.*, *141*, 477–508, doi:10.1007/s11214-008-9433-1.

Ozeke, L. G., and I. R. Mann (2001), Modeling the properties of high-*m* Alfvén waves driven by the drift-bounce resonance mechanism, *J. Geophys. Res.*, *106*(A8), 15,583–15,597, doi:10.1029/2000JA000393.

Ozeke, L. G., and I. R. Mann (2005), High and low ionospheric conductivity standing guided Alfvén wave eigenfrequencies: A model for plasma density mapping, *J. Geophys. Res.*, *110*, A04215, doi:10.1029/2004JA010719.

Plaschke, F., K.-H. Glassmeier, H. U. Auster, V. Angelopoulos, O. D. Constantinescu, K.-H. Fornaçon, E. Georgescu, W. Magnes, J. P. McFadden, and R. Nakamura (2009), Statistical study of the magnetopause motion: First results from THEMIS, *J. Geophys. Res.*, *114*, A00C10, doi:10.1029/2008JA013423.

Poulter, E. M., W. Allan, E. Nielsen, and K.-H. Glassmeier (1983), STARE radar observations of a Pg pulsation, *J. Geophys. Res.*, *88*, 5668–5676, doi:10.1029/JA088iA07p05668.

Radoski, H. R. (1967), Highly asymmetric MHD resonances: The guided poloidal mode, *J. Geophys. Res.*, *72*(15), 4026–4027.

Radoski, H. R., and R. L. Carovillano (1966), Axisymmetric plasmasphere resonances: Toroidal mode, *Phys. Fluids*, *9*(2), 285−291.

Rostoker, G., H. L. Lam, and J. V. Olson (1979), Pc4 giant pulsations in the morning sector, *J. Geophys. Res.*, *84*(A9), 5153–5166.

Russell, C. T., P. J. Chi, D. J. Dearborn, Y. S. Ge, B. Kuo-Tiong, J. D. Means, D. R. Pierce, K. M. Rowe, and R. C. Snare (2008), THEMIS ground-based magnetometers, *Space Sci. Rev.*, *141*(1–4), 389–412, doi:10.1007/s11214-008-9337-0.

Sarris, T. E., et al. (2009), Characterization of ULF pulsations by THEMIS, *Geophys. Res. Lett.*, *36*, L04104, doi:10.1029/2008GL036732.

Shue, J.-H., et al. (1998), Magnetopause location under extreme solar wind conditions, *J. Geophys. Res.*, *103*(A8), 17,691–17,700.

Sibeck, D. G., G. I. Korotova, D. L. Turner, V. Angelopoulos, K.-H. Glassmeier, and J. P. McFadden (2012), Frequency-doubling and field-aligned ion streaming in a long-period poloidal pulsation, *J. Geophys. Res.*, *117*, A11215, doi:10.1029/2011JA017473.

Singer, H. J., and M. G. Kivelson (1979), The latitudinal structure of Pc5 waves in space: Magnetic and electric field observations, *J. Geophys. Res.*, *84*, 7213–7222.

Singer, H. J., J. W. Hughes, and C. T. Russell (1982), Standing hydromagnetic waves observed by ISEE 1 and 2: Radial extent and harmonic, *J. Geophys. Res.*, *87*(A5), 3519–3529.

Singer, H. J., L. Matheson, R. Grubb, A. Newman, and S. D. Bouwer (1996), Monitoring space weather with the GOES magnetometers, *GOES-8 and Beyond*, *Proc. SPIE Int. Soc. Opt. Eng.* (2812), 299–308.

Southwood, D. J. (1974), Some features of field line resonances in the magnetosphere, *Planet. Space Sci.*, *22*, 483–491.

Southwood, D. J. (1976), A general approach to low-frequency instability in the ring current plasma, *J. Geophys. Res.*, *81*(19), 3340–3348.

Southwood, D. J., and M. G. Kivelson (1982), Charged particle behavior in low-frequency geomagnetic pulsations, 2, Graphical approach, *J. Geophys. Res.*, *87*(A3), 1707–1710.

Southwood, D. J., and M. G. Kivelson (1997), Frequency doubling in ultralow frequency wave signals, *J. Geophys. Res.*, *102*(A12), 27,151–27,158.

Southwood, D. J., J. W. Dungey, and R. J. Etherington (1969), Bounce resonant interaction between pulsations and trapped particles, *Planet. Space Sci.*, *17*(3), 349–361.

Sugiura, M., and C. R. Wilson (1964), Oscillation of the geomagnetic field lines and associated magnetic perturbations at conjugate points, *J. Geophys. Res.*, *69*(7), 1211–1216.

Takahashi, K., and R. L. McPherron (1984), Standing hydromagnetic oscillations in the magnetosphere, *Planet. Space Sci.*, *32*, 1343–1359.

Takahashi, K., R. L. McPherron, and T. Terasawa (1984), Dependence of the spectrum of Pc3-4 pulsations on the interplanetary magnetic field, *J. Geophys. Res.*, *89*, 2770–2780.

Takahashi, K., J. F. Fennell, E. Amata, and P. R. Higbie (1987), Field-aligned structure of the storm time Pc5 wave of November 14-15, 1979, *J. Geophys. Res.*, *92*(A6), 5857–5864.

Takahashi, K., N. Sato, J. Warnecke, H. Lühr, H. E. Spence, and Y. Tonegawa (1992), On the standing wave mode of giant pulsations, *J. Geophys. Res.*, *97*(A7), 10,717–10,732.

Takahashi, K., R. E. Denton, and D. Gallagher (2002), Toroidal wave frequency at L = 6–10: Active Magnetospheric Particle Tracer Explorers/CCE observations and comparison with theoretical model, *J. Geophys. Res.*, *107*(A2), 1020, doi:10.1029/2001JA000197.

Takahashi, K., K.-H. Glassmeier, V. Angelopoulos, J. Bonnell, Y. Nishimura, H. J. Singer, and C. T. Russell (2011), Multisatellite observations of a giant pulsation event, *J. Geophys. Res.*, *116*, A11223, doi:10.1029/2011JA016955.

Thompson, S. M., and M. G. Kivelson (2001), New evidence for the origin of giant pulsations, *J. Geophys. Res.*, *106*(A10), 21,237–21,253.

Tsyganenko, N. A. (1989), A magnetospheric magnetic field model with a warped tail current sheet, *Planet. Space Sci.*, *37*, 5–20.

Vaivads, A., W. Baumjohann, G. Haerendel, R. Nakamura, H. Kucharek, B. Klecker, M. R. Lessard, L. M. Kistler, T. Mukai, and A. Nishida (2001), Compressional Pc5 type pulsations in the morning plasma sheet, *Ann. Geophys.*, *19*, 311–320.

Wilson, M. E., T. K. Yeoman, L. J. Baddeley, and B. J. Kellet (2006), A Statistical investigation of the invariant latitude dependence of unstable magnetospheric ion populations in relation to high *m* ULF wave generation, *Ann. Geophys.*, *24*, 3027–3040.

Wright, D. M., and T. K. Yeoman (1999), High-latitude HF Doppler observations of ULF waves: 2, Waves with small spatial scale sizes, *Ann. Geophys.*, *17*, 868–876.

Yang, B., Q.-G. Zong, Y. F. Wang, S. Y. Fu, P. Song, H. S. Fu, A. Korth, T. Tian, and H. Reme (2010), Cluster observations of simultaneous resonant interactions of ULF waves with energetic electrons and thermal ion species in the inner magnetosphere, *J. Geophys. Res.*, *115*, A02214, doi:10.1029/2009JA014542.

Yeoman, T. K., and D. M. Wright (2001), ULF waves with drift resonance and drift-bounce resonance energy sources as observed in artificially-induced HF radar backscatter, *Ann. Geophys.*, *19*, 159–170.